Available online at www.sciencedirect.com
SCIENCE DIRECT®
Acta Materialia 52 (2004) 1837–1845
Acta MATERIALIA
www.actamat-journals.com

# Large deformation of living cells using laser traps

C.T. Lim [a,b], M. Dao [a,*], S. Suresh [a], C.H. Sow [c], K.T. Chew [b]

[a] Department of Materials Science and Engineering, Massachusetts Institute of Technology, 77 Massachusetts Ave., Rm 8-139, Cambridge, MA 02139, USA
[b] Division of Bioengineering and Department of Mechanical Engineering, The National University of Singapore, Singapore 117576, Singapore
[c] Department of Physics, The National University of Singapore, Singapore 117576, Singapore

Received 17 November 2003; received in revised form 13 December 2003; accepted 15 December 2003

**Abstract**

We present experimental results of large deformation of human red blood cells subjected to direct stretching by optical tweezers. The maximum external force imposed on the cell is in excess of 400 pN. A three-dimensional computational simulation of the biconcave cell membrane is also performed to extract the large deformation elastic properties from the experimental results obtained during loading as well as upon relaxation of the load. Different constitutive formulations of the cell membrane with its underlying spectrin network are explored in the computational simulations in an attempt to investigate the mechanical response and to compare the results so obtained with those derived from other independent experimental techniques. These results demonstrate new capabilities in the use of optical tweezers for study of cell deformation at large strains and provide a framework to explore possible effects of different loading configurations, disease states, chemical factors and environment on the large deformation characteristics of biological cells.


*Keywords:* Optical traps; Biological cells; Human red blood cell; Elastic behavior; Viscoelasticity

## 1. Introduction

Laser traps or laser tweezers, also commonly known as optical traps or optical tweezers, are finding increasingly widespread applications in the study of mechanical deformation of isolated biological cells and molecules (see [1], for example). In this method a laser beam, which is focused through a microscope objective lens, attracts and traps a high refractive index particle, and deformation is induced as the particle attached to a cell or a molecule moves with the beam. The range of forces that can be imposed by the optical trap is typically on the order of tens of pico-Newton ($\mathrm{pN} = 10^{-12}$ N) as, for example, that employed previously to study human red blood cell [2–4]. Many important phenomena in biology, such as cell deformation and protein unfolding, require mechanical forces which are significantly larger than those typically obtained by optical tweezers so that real mechanistic phenomena can be properly simulated and analysed by inducing sufficient deformation. In fact, forces in the range of a few hundred pico-Newton have been achieved with the optical trap technique in a study of the unfolding of titin molecule [5] although, to date, such high forces do not appear to have been employed for the study of large deformation of the single cell.

Consider the human red blood cell (erythrocyte), with diameter 7–8.5 μm, which undergoes severe elastic deformation during passage through narrow capillaries smaller than about 3 μm in diameter. The cell membrane, which consists of the phospholipid bilayer supported underneath by a spectrin network, is primarily responsible for such large deformation [6–15]. Investigating how red cells deform provides insights into their physiology, cell biology and biorheology. Establishing possible connections between mechanical properties of red blood cell membrane and diseases such as malaria or sickle cell anaemia is also a subject of considerable scientific interest; see, for example [16].

In the conventional micropipette aspiration method [8–13], the cell membrane is deformed through entry

* Corresponding author. Tel.: +1-617-253-2100; fax: +1-208-248-5818.
*E-mail address:* mingdao@mit.edu (M. Dao).

1359-6454/$30.00 © 2004 Acta Materialia Inc. Published by Elsevier Ltd. All rights reserved.
doi:10.1016/j.actamat.2003.12.028

into a micropipette by suction. By monitoring the attendant geometry changes from optical images, the elastic response of the membrane is inferred while neglecting the effects of any edge stress concentration or internal wall friction of the micropipette. This method has implied in-plane shear modulus values of 4–10 μN/m for the cell membrane [8,13]. Although commonly used for studying the deformation of living cells, the micropipette aspiration technique imposes a complex stress state on the cell, which can pose considerable challenge in the interpretation of the mechanical response. Atomic force microscopy [14,17] along with elastic contact theory of deformation has also been attempted to estimate mechanical properties of the cell, despite complications involving complex states of stress and deformation.

Optical tweezers allow for direct stretching of the cell in one or more directions by trapping beads that are strategically attached to the cell surface. Recent studies have employed this method for the study of red blood cells with a stretching force smaller than 60 pN, which is insufficient to induce sufficiently large deformation. In addition, interpretations of deformation induced by optical tweezers using linear elastic analysis [2–4,18,19] are incapable of capturing accurately the severe deformation characteristics of the cell membrane. Furthermore, these initial experimental studies have not provided complete deformation characteristics of the cell in that both the axial and transverse diameter changes (and hence the complete deformation responses) have not been systematically documented in the experiments. The relaxation characteristics of the deformed red blood cell upon release of the stretching force also have not been examined systematically in the optical tweezers experiments. There is a critical need to develop newer and more refined experimental tools to study the deformation characteristics under different stress states in order to explore connections among the mechanical, chemical and biological characteristics of living cells.

Here, we demonstrate use of optical tweezers to study the deformation characteristics of the human red blood cell with stretching forces nearly an order of magnitude larger than those achieved previously with optical tweezers for the human red blood cell. We further provide new experimental results of the viscoelastic response obtained from the relaxation characteristics. These results, in conjunction with three-dimensional computational simulations, provide a powerful framework with which the elastic and viscoelastic deformation characteristics of living cells can be studied. The companion paper [20] further discusses the mechanics of large deformation of the cell by optical tweezers.

## 2. Experimental method

We have performed large deformation experiments on the human red blood cell by directly stretching the cell to forces in excess of 400 pN using optical tweezers as described below. The experimental apparatus was carefully designed and calibrated to ensure accuracy and reproducibility of measurements. The key components of this set up consist of a 1.5 W diode-pumped Nd:YAG laser source (Cell Robotics, Albuquerque, NM) connected to an inverted microscope (Leica Microsystems, Wetzlar, Germany). The laser beam was used to trap high refractive-index silica beads attached diametrically across the cell periphery. The silica microbeads used were 4.12 μm in diameter. The images of the red cell were captured from the microscope using a CCD camera and recorded onto a videotape. The video images were then downloaded onto a computer and digitized for image analysis. As the original and stretched diameters of a human red blood cell fell in the range 4.5–16 μm, the calibration and the measurements were carried out using the digitized video images with a resolution of 100 nm per pixel on the viewing screen. A copper grid with periodic array of square holes was used to calibrate the actual size of the field of view under the microscope.

The calibration technique involved inducing a flow of the buffer solution across the trapped bead at an increasing rate until the bead became dislodged from the optical trap. Calibration of the optical trapping force at a number of specified laser power settings was carried out on silica microbeads (Bangs Laboratories, Fisher, IN) with diameters of 4.12 μm in a PBS (phosphate-buffered saline) solution. The maximum force $F$ that can be sustained by the laser is evaluated using Stokes' Law

$$F = \beta v, \tag{1}$$

where $\beta$ is the viscous drag coefficient and $v$ is the velocity of flow across the microbead at the point when the bead was just about to be dislodged from the laser trap. The viscous drag coefficient $\beta$ of a bead with radius $r$ whose center is a distance $h$ from the surface is [21]:

$$\beta = \frac{6\pi\eta_f r}{\left[1 - \frac{9}{16}\left(\frac{r}{h}\right) + \frac{1}{8}\left(\frac{r}{h}\right)^3 - \frac{45}{256}\left(\frac{r}{h}\right)^4 - \frac{1}{16}\left(\frac{r}{h}\right)^5\right]}, \tag{2}$$

where $\eta_f$ is viscosity of fluid (PBS). For the force calibration, $h/r > 5$ was used for the trapped bead so as to minimize the effect of drag due to distance of the bead from the cover-glass surface. Using a Rheometric fluid spectrometer (Rheometrics Scientific, Piscataway, NJ), the viscosity of the PBS solution was measured to be $\eta_f = 0.00898$ Pa s. A flow chamber, of dimensions 30 mm × 5 mm × 200 μm, was used to conduct this calibration experiment.

Two glass tubes attached at both ends of the flow chamber were used to provide the flow of PBS solution across the trapped bead. The flow velocity $v$ at which the trapped bead was just on the verge of escaping from the laser trap (see Fig. 1) was inferred from the free flowing

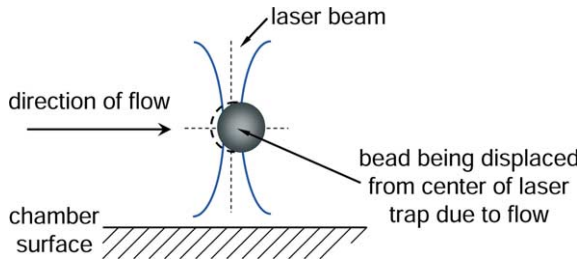


Fig. 1. Schematic illustration of the trapped bead which is just on the verge of escaping from the optical trap. The bead is being displaced slightly away from the focus of the laser beam.

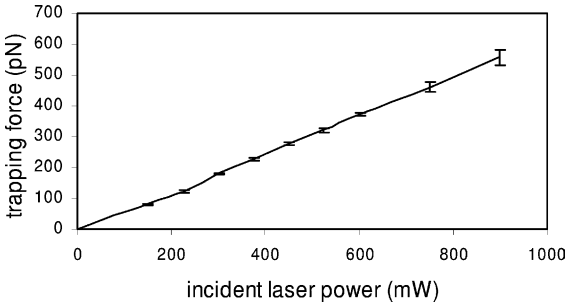


Fig. 3. Force calibration plot showing the variation of trapping force with laser power for a 1.5 W diode pumped Nd:YAG laser source for the single optical trap system. The standard deviation in the force values obtained from three separate calibration tests is less than 5.2%.

beads in the PBS solution. From the image analysis as shown in Fig. 2, we were able to measure the distance travelled by individual flowing beads in the background in two successive frames right at the point when the trapped bead had just become dislodged from the trap. With the measured distance and the frame rate known, the flow velocity of PBS could then be calculated; see Figs. 1 and 2. The effective image recording rate was 50 frames/s. Similar calibration methods have been employed in recent optical tweezers studies of red blood cell deformation at lower stretching force (for example, [2,3]) and of the unfolding of titin molecule at high stretching force [5]. Although other calibration methods [1] have been employed for force determination as a function of input laser power for optical traps, it should be noted that the current calibration method is the preferred technique for mechanical deformation of single cells [2,3] and for molecules at large external force [5].

The force calibration plot obtained from three sets of repeat calibration experiments is shown in Fig. 3. This calibration plot showing trapping force as a function of laser power was found to be highly reproducible; the standard deviation in the force values was less than 5.2%. Cell stretching experiments were carried out immediately after completion of force calibration. Two silica microbeads (diameter 4.12 μm, Bangs Laboratories, Fisher, IN) that were non-specifically attached diametrically across the cell surface were used as "grips" to stretch the cell. The method of attaching silica microbeads to the cell was similar to that of Henon et al. [2]. Blood samples were obtained from a healthy adult male. All preparations were made at room temperature. At least eight different cell samples were studied and the changes in both axial and transverse diameters were recorded. The typical scatter observed in the stretching experiments are reported here along with the average diameter changes.

In the stretching experiment conducted at room temperature, one of the two microbeads was adhered to the glass surface, while the other was trapped using the laser beam. The cell was then stretched by moving the sample chamber on the stage of the microscope relative to the focused laser beam. The sample stage moved continuously until the bead became dislodged, when the preset maximum trapping force could no longer sustain the stretched blood cell. This is schematically illustrated in Fig. 4.

Other possible sources of error were also carefully examined. No significant deviation in the position of the

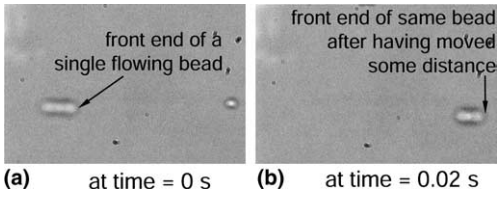


Fig. 2. The distance travelled by individual flowing beads in the background were measured using two successive frames of the video-image right at the point when the trapped bead had just become dislodged from the trap. The distance travelled by the free flowing bead was measured by locating how much the front end of the bead had moved within the two frames. Knowing that the time between successive frames was 0.02 s (recording rate was 50 frames/s), the flow velocity of PBS could then be calculated.

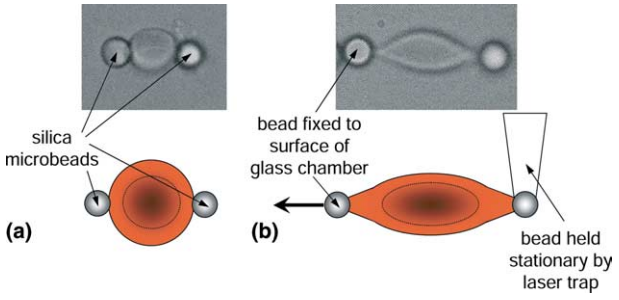


Fig. 4. Illustration of the optical trap method. (a) Two silica microbeads, each 4.12 μm in diameter, are non-specifically attached to the red cell at diametrically opposite points. The left bead is anchored to the surface of the glass slide. The optical image corresponds to the unstrained configuration. (b) The right bead is trapped using the optical tweezers and the cell is then stretched by moving chamber where the left bead is attached. The trapped bead remains stationary. The optical image shows an example of the ensuing large deformation of the cell.

trapped beads was found perpendicular to the plane of observation. The size of trapping laser beam at the focal point was less than 1 μm in diameter, which was significantly smaller than the 4.12 μm bead size. Further, as the stretching of the cell was achieved in a short time period of only 2–5 s, the possibility of any significant heating of the bead or the cell membrane is considered circumvented.

## 3. Theoretical consideration and computational simulation

### 3.1. Constitutive model

The membrane of the cell, which includes the phospholipid bilayer, the transmembrane protein structures and spectrin network, can be represented by an effective thin shell. In the widely used approach, the cell membrane is modelled as incompressible [8,22] where the relation between the membrane shear stress $T_s$ (expressed in units of force per unit length) and deformation is

$$T_s = 2\mu\gamma_s = \frac{\mu}{2}(\lambda_1^2 - \lambda_2^2), \tag{3a}$$

$$T_s = \tfrac{1}{2}(T_1 - T_2) \quad \text{and} \quad \gamma_s \equiv \tfrac{1}{2}(\varepsilon_1 - \varepsilon_2) = \tfrac{1}{4}(\lambda_1^2 - \lambda_2^2), \tag{3b}$$

$$\lambda_1\lambda_2 = 1, \tag{3c}$$

where $T_1$ and $T_2$ are the in-plane principal membrane stresses, $\varepsilon_1$ and $\varepsilon_2$ are the in-plane principal Green's strains of the membrane, $\lambda_1$ and $\lambda_2$ are the principal stretch ratios, $\mu$ is the membrane shear modulus (assumed to be constant and expressed in units of force per unit length) and $\gamma_s$ is the shear strain. Note that Eq. (3c) signifies the assumption of a constant area for the cell membrane. If the deformation were uniform, the stretch ratios $\lambda_1$ and $\lambda_2$ approximately would represent the ratios of the current diameters to the initial diameters in the axial and transverse direction of the cell, respectively. However, in the micropipette aspiration, atomic force microscopy and optical trap techniques, the deformation is nonuniform. The constitutive model described in Eq. (3) has been the basis for interpreting the mechanical response of the red blood cell in many experimental studies that employed the micropipette aspiration technique [8,22].

Other possible constitutive models can also be explored in the context of the deformation of red blood cells. One such approach entails use of a hyperelastic effective material model for capturing the large deformation response of the membrane. The simplest first order formulation in this case invokes the assumption of incompressibility (constant volume) where the strain energy potential function [23] is of the form,

$$U = \frac{G_0}{2}(\lambda_1^2 + \lambda_2^2 + \lambda_3^2 - 3), \tag{4}$$

where $G_0$ is the initial value of bulk shear modulus, and $\lambda_i$ ($i = 1$ to 3) are the principal stretches. The incompressibility condition implies that $\lambda_1\lambda_2\lambda_3 = 1$. The potential function $U$ defines the nonlinear elastic stress–strain behavior. When the initial membrane thickness is $h_0$ the constitutive description of Eq. (4) results in the initial in-plane membrane shear modulus $\mu_0 = 0.75G_0h_0$. Fig. 5(a) schematically shows the uniaxial stress–strain response of such a neo-Hookean hyperelastic material, the membrane elasticity modulus typically decreases from its initially high value, $\mu_0$ to a relatively smaller value, $\mu_l$ at larger strains, before attaining a higher value, $\mu_f$ again prior to final failure. The slope of the membrane shear stress ($T_s$) versus shear strain ($2\gamma_s$) is therefore a decreasing function of shear strain (see Fig. 5(b)). For the simple first order neo-Hookean material described by Eq. (4), only the first stage ($\mu_0$) and the second stage ($\mu_l$) will be considered subsequently. Specifically, $\mu_l$ is taken here at a relatively large stretch ratio of $\lambda_1 = 3$ under direct uniaxial tension. As shown later, the strain values introduced in the cell membrane during large deformation in the present optical trap experiments correspond to the intermediate region of the stress–strain curve in Fig. 5(a) where the membrane shear modulus is close to $\mu_l$. Thus, the neo-Hookean rubber elasticity model for the membrane entails two material parameters: the initial shear modulus $\mu_0$ and the second stage, large deformation modulus $\mu_l$. In the current first order model, choice of one value of the two parameters also determines the other; while introducing higher order terms will result in independent variations of $\mu_0$ and $\mu_l$. Choice of values of both of these parameters which facilitate the matching of computational predictions with experimental results have been systematically explored, and reported in this paper and in [20].

When the constant membrane area constraint, i.e., $\lambda_1\lambda_2 = 1$ (i.e., $\lambda_3 = 1$), is added to Eq. (4), the constitu-

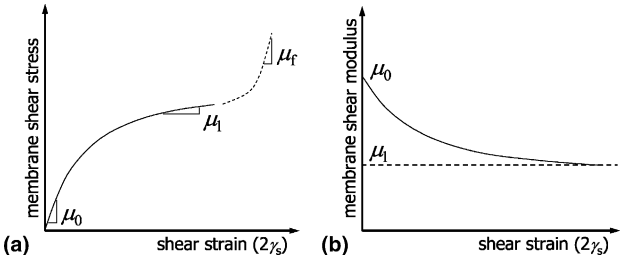


Fig. 5. Schematic illustration of the hyperelastic constitutive response used in some of the computational simulations. (a) Uniaxial stress–strain response. (b) The variation of the membrane shear modulus with the progression of deformation in the early region and in the in-between region, where strains are representative of the large deformation response achieved in the present optical tweezer experiments. The final deformation regime with the shear modulus of $\mu_f$ is not shown in this figure.

tive description of Eq. (4) is equivalent to that of Eq. (3). With this additional constraint, the in-plane membrane shear modulus stays at a constant value of $\mu = G_0 h_0$ throughout the entire deformation history.

While the foregoing analytical descriptions for the thin shell employ a single material property, i.e., the membrane shear modulus, more comprehensive analyses involving computational simulations of cell deformation invoke another material parameter in addition to the in-plane shear modulus $\mu$: the bending modulus $B$. Taking the literature values of $B$ to be $1–9 \times 10^{-19}$ N m [3,24], the contribution from the bending modulus is found to be relatively much smaller. Therefore, a typical (fixed) value of $B = 2 \times 10^{-19}$ N m is assumed in all the computations unless specified otherwise. By matching the computational simulations with experimentally observed shape during large deformation, shear modulus can be extracted on the basis of the foregoing constitutive assumptions.

The cytosol is assumed to be a fluid which acts to preserve the internal volume of the red blood cell during deformation. The viscous energy dissipation of the cytoplasm within the red cell filled with concentrated haemoglobin solution is known to be two orders of magnitude smaller than that of the membrane [25]; therefore the viscosity of the cytosol is ignored although the presence of the fluid is simulated in all numerical models. The volume of the fluid inside the cell was assumed to be constant in all the simulations.

### 3.2. Computational model

Simulation of cell membrane deformation was performed using the finite element method where the membrane comprising the phospholipid bilayer and the spectrin network was assumed to be an effective continuum as discussed above. The force was applied at diametrically opposite ends of the cell. The rigid silica beads were assumed to be attached to the cell over a small oval region of 1–2 μm in diameter so that final contact conditions could be properly simulated. A fully three-dimensional model of the biconcave cell was constructed using an averaged shape estimated from experiment [19,26], where the initial diameter of the cell was taken to be 7.82 μm. Only half of the cell was simulated using symmetric boundary conditions with 12,000 three-dimensional shell elements in the finite element program, ABAQUS [27]. Details of the mechanics of deformation including details of the computational method are provided in [20].

## 4. Results

When the applied force is smaller than 20–30 pN, the cell undergoes small elastic deformation (Fig. 6) and in this regime, our results are similar to those reported previously in the literature [2]. Large deformation behavior begins at a stretching force of about 30 pN. Based on the change in transverse diameter obtained from our experiment and using Eq. (4) in Henon et al. [2], the in-plane shear modulus of the erythrocyte membrane is found to be approximately 2.5 μN/m for stretching force below 30 pN. Hence, our shear modulus estimate is within the range of values estimated in prior work based on the optical tweezers method [2–4] for small deformation of the red blood cell. This also validates our testing methodology on the basis of which newer experiments on large deformation were initiated.

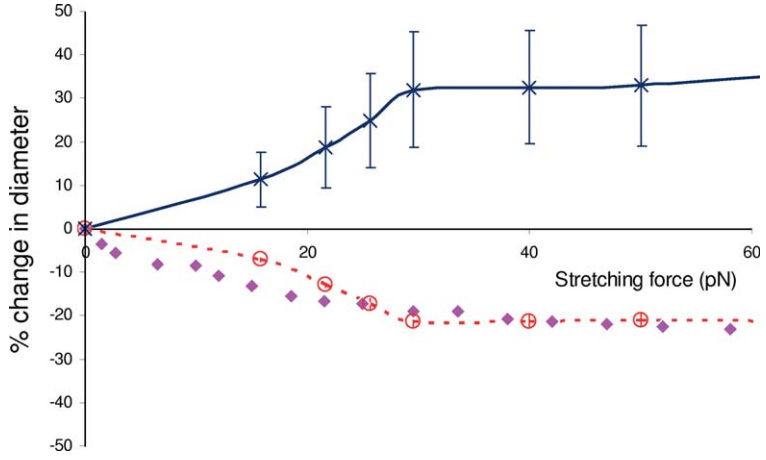


Fig. 6. Experimentally determined variation of the axial (×) and transverse (○) diameters of the red cell as a function of stretching force at small deformation from the present study. The scatter in the axial diameter, shown here based on six repeat experiments on different cells, is significantly larger than that observed in the transverse diameter. Our experiments show that the transition from small deformation to large deformation occurs at approximately 30 pN. The change in transverse diameter compares well with that previously reported by Henon et al. [2] based on their discotic model (◆). Prior studies [2] did not report changes in the axial diameter as functions of stretching force.

Fig. 7 shows that the observed shape changes are well matched by computation for which $\mu_l$ was assumed to be 13.3 μN/m (with $\mu_0 = 22.5$ μN/m). The contact size, $d_c$ was taken to be 2 μm in this set of calculations. The left column in the figure is a sequence of optical images revealing large deformation response of the red blood cell at different stretching forces. At 340 pN, the axial diameter of the cell increases by 50% and the transverse diameter is reduced by more than 40%. The middle column shows contours of constant maximum principal strain at corresponding stretching forces; logarithmic strains at sites of contact between the cell and the beads can reach values of approximately 100% at a stretching force of 340 pN. The right column shows one half of the computed full three-dimensional shape of the cell at different imposed forces; the structural folding observed at large strains appears to contribute significantly towards the rapid shrinking in the transverse direction.

Comparisons of predicted and measured changes in axial and transverse diameters of the cell are plotted in Fig. 8 for $\mu_l = 11$ and 18 μN/m (with $\mu_0 = 19$ and 30 μN/m, respectively). Again the contact size $d_c$ was taken to be 2 μm. Simulations capture experimental trends over the full range of large deformation. Video images of both experiment and computation can be seen in the supplementary information provided with the electronic archive of [20]. In the computational video images, the existence of the cytosol inside the membrane prevents contact between the upper and lower surfaces; some folding and rotation of the cell membrane, are also observed which can be seen in the right column of Fig. 7. Although quantitative comparison of this effect with experiment is not feasible because of the paucity of three-dimensional imaging of the deforming cell, it is evident that large deformation induces severe configurational changes which can lead to apparent changes in effective structural rigidity.

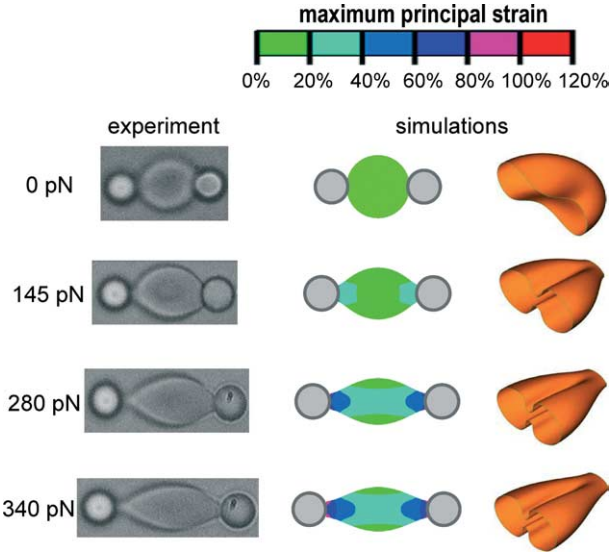


Fig. 7. Images of the red cell being stretched from 0 to 340 pN. The images in the left column are obtained from experimental video photography whereas the images in the center column (top view) and in the right column (half model 3D view) correspond to large deformation computational simulation of the biconcave red cell (with $\mu_l = 13.3$ μN/m, $\mu_0 = 22.5$ μN/m). The middle column shows a plan view of the stretched biconcave cell undergoing large deformation at the forces indicated on the left. The predicted shape changes are in reasonable agreement with observations. The color contours in the middle column represent spatial variation of constant maximum principal strain. The right column shows one half of the full three-dimensional shape of the cell at different imposed forces; here, the membrane was assumed to contain a fluid, which preserved the internal volume.

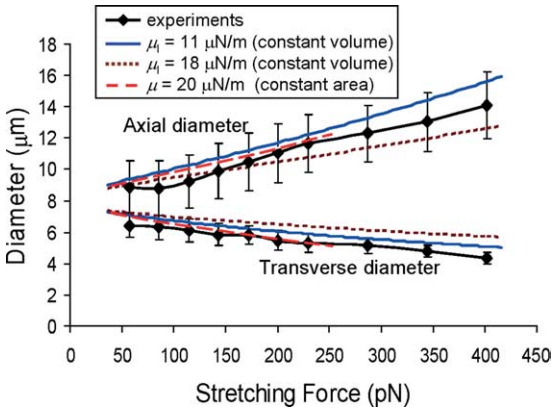


Fig. 8. Variation of measured axial and transverse diameter (solid line with scatter band) of red cell against stretching force of optical tweezers during large deformation. The solid and dotted lines represent computational predictions for the axial/transverse diameter with $\mu_l = 11$ and 18 μN/m, and with $\mu_0 = 19$ and 30 μN/m, respectively, invoking the hyperelastic constitutive response, Eq. (4), which assumes constant volume. The computational model uses the three-dimensional biconcave disk with a contact diameter of 2 μm. Also shown are the predictions of simulations assuming constant membrane area, represented by long dashed lines, using the model given by Eq. (3).

The in-plane shear modulus $\mu_l = 11$ to 18 μN/m estimated by our analysis using the constitutive description of Eq. (4) for large deformation with optical tweezers is somewhat higher than the range of values, 4–10 μN/m, estimated on the basis of the micropipette aspiration experiments [19,22] where the stress state and loading mode are significantly different from those of the present experiments. Alternatively, if we invoke the constitutive response given in Eq. (3) with constant area for the cell membrane in our three-dimensional computational simulation, a fixed value of the membrane shear modulus, $\mu_0 = \mu_l = \mu_f$ 20 μN/m appears to match the average values of our experimental observations of variations in axial and transverse diameter of the cell with the applied force (see Fig. 8). It is interesting to note that, in their optical tweezers experiments on human red blood cell membranes subject to maximum forces of 15 pN, Sleep et al. [3] report membrane shear modulus values as high as 200 μN/m, which is an order of magnitude higher than that estimated from micropi-

pette aspiration experiments. Sleep et al. [3] note that the membrane shear modulus from micropipette aspiration is lower than their optical trap results. They postulate that the aspiration of the cell may have resulted in an effective phase separation caused by the accumulation of the integral membrane proteins at the entrance to the capillary instead of following the membrane flow into the micropipette [28].

When the stretching force imposed by the optical tweezers is released at the point of maximum deformation, the cell returns to its original shape. The elastic relaxation response during this recovery phase can be also exploited to infer the viscoelastic properties of the cell membrane. Adding the viscoelastic term to the constitutive behavior of the cell membrane, Eq. (3) can be modified as [25],

$$T_s = \frac{\mu}{2}(\lambda_1^2 - \lambda_1^{-2}) + 2\eta\frac{\partial ln\lambda_1}{\partial t}, \tag{5a}$$

$$t_c = \frac{\eta}{\mu}, \tag{5b}$$

where $\eta$ is the coefficient of surface viscosity of the cell membrane, $t$ is time, and $t_c$ is the characteristic time for relaxation.

On the basis of this equation, Hochmuth et al. [12] proposed a simple expression to calculate the recovery characteristic time $t_c$

$$\frac{(\lambda_1^2 - 1)(\lambda_{1,max}^2 + 1)}{(\lambda_1^2 + 1)(\lambda_{1,max}^2 - 1)} = \exp\left(-\frac{t}{t_c}\right), \tag{5c}$$

where $\lambda_{1,max}$ is the initial (maximum) value of the stretch ratio of the red cell. Fig. 9 shows the corresponding best fit to the experimental data on relaxation using Eq. (5c). Using relaxation data from eight different experiments, the characteristic time is estimated to be $t_c = 0.19 \pm 0.06$ s, which is slightly higher than the value of 0.10–0.13 s estimated from micropipette aspiration experiments. Taking estimated membrane shear modulus $\mu$ to be approximately 13 μN/m, the corresponding membrane viscosity, $\eta$, calculated from Eq. (5b) and Fig. 9 is about 1.7–3.3 (μN/m) s, which compares well with the literature values of 0.6–2.7 (μN/m) s found using micropipette experiments [24]. We also performed three-dimensional computational simulations of the loading response by incorporating the viscoelastic term on the right hand side of Eq. (5a). Taking $t_c = 0.19$ s and an estimated stretch rate on the order of $\dot{\lambda}_1 = 0.3\ s^{-1}$ in the current study, the error caused by ignoring membrane viscosity during the loading stage is found to be negligibly small. Thus the results in Fig. 8 appear to capture reasonably the overall large deformation loading response of the cell membrane even though the viscoelastic factor is not considered there.

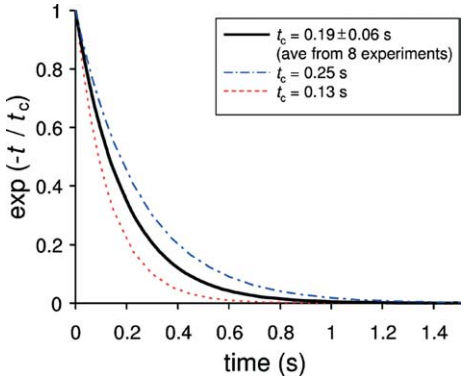


Fig. 9. Best fit to the experimental relaxation data. Using relaxation data from eight different experiments, the characteristic time was estimated to be $t_c = 0.19 \pm 0.06$ s using Eq. (5c).

## 5. Discussion

We have reported the experimental results of large deformation induced by direct stretching using the optical tweezers. The new experimental and computational tools developed in this work collectively provide a powerful framework with which possible effects of such factors as disease state, cholesterol, drugs, and environment (for example, cigarette smoke, pollution) on large deformation of cells can be explored for diagnostics and treatment. In this context, it is of interest to note that experimental studies using optical tweezers have also been performed recently to measure red cell membrane elasticity after controlled exposure to the malaria parasite, *Plasmodium falciparum* [29]. These studies have shown the feasibility of accurately and systematically measuring the changes in membrane deformation capability as a function of time of infestation of the red blood cell with the parasites. They also point to the opportunities for establishing possible direct connections between the deformation characteristics of living cells and the progression of diseases. It is widely considered [16] that proteins exported from the parasites interact with the red blood cell membrane skeleton and alter its physical properties which, in turn, result in the progression of the disease. Our preliminary experiments [29] reveal that the changes in the elastic properties of the red blood cell membrane can be monitored in a controlled manner by recourse to the optical tweezers technique outlined here for probing both small and large deformation characteristics. The ability of the optical tweezers technique to allow for full control on the extent of deformation of cell membrane gives it an added significant advantage over existing methods. This versatility of the optical tweezers which allows the application of not only varying loads but also multiple point loading (through the use of multiple traps) makes it an attractive technique for investigating the deformation of biological cells.

The change in the axial diameter plotted in Fig. 8 shows considerable scatter, which may be attributed to several factors. The life span of a red blood cell in the body is about 120 days; different samples tested may be at different stages of their life span. Exact locations at which the beads are attached to the cell, which cannot be precisely controlled, and finite contact areas may affect the cell response. Small variations in the initial size and shape of the erythrocyte may also contribute to the observed scatter.

The discussion here on the deformation characteristics of the red blood cell membrane has been based on continuum formulations. It should be noted that approaches involving coarse-grained molecular models of the cell membrane spectrin network have also been employed to study the large deformation characteristics of red blood cells. Computations have been carried out using Monte Carlo simulations on a biconcave-shaped spectrin cytoskeleton network [30,31]. Such simulations were performed in conjunction with the micropipette aspiration experiments where the modulus values were found to be consistent with the experimentally extracted ones of 6–9 μN/m. More recently, spectrin-network level computational models [32] simulating the deformation of spectrin nodes that surround the cytosol of the red blood cell have also been performed to determine diameter changes under unidirectional stretching induced by optical tweezers. These models reveal effective membrane shear modulus value of approximately 20 μN/m [32].

## 6. Conclusions

1. Direct stretching of a human red blood cell under large deformation has been demonstrated using laser tweezers for biological cells. The maximum stretching force imposed on the cell was in excess of 400 pN, nearly an order of magnitude higher than that achieved previously for deforming the red blood cell using laser tweezers.
2. Three-dimensional finite element model of the actual biconcave shape of a human red blood cell were constructed and comprehensive computational studies were performed using the newly constructed model. The three-dimensional biconcave model matches the experimental results in both axial and transverse directions for direct stretching of the blood cell. The spherical model employed in earlier studies [2,3] on small deformation of red blood cells was shown to be able to fit only one direction well.
3. Systematic experiments of the relaxation response of the red blood cell following large deformation stretch by optical tweezers have also been performed. The characteristic relaxation time from such experiments was estimated using a simple viscoelastic model and was shown to be in the range 0.13–0.26 s, compared to the value of 0.10–0.13 s extracted from the micropipette aspiration method.
4. Taking the literature values of the bending modulus to be $1–9 \times 10^{-19}$ N m, the contribution from the bending modulus to the overall deformation is found to be nearly negligible, especially at large strains.
5. The large deformation elastic response of the cell was determined in the present work using several different constitutive models. When the three-dimensional computational simulations of cell deformation, which take into account the biconcave shape, a volume-preserving fluid medium (cytosol) in the cell interior, and realistic contact conditions for the beads used in the optical tweezers, are used in conjunction with a hyperelastic constitutive model, the membrane shear modulus values are found to be in the range 11–18 μN/m at average strains typical of large deformation while initial shear modulus values in the range 19–30 μN/m. The literature values of 4–10 μN/m at comparable strain levels are extracted primarily from micropipette aspiration experiments, which entail a very different stress state and boundary conditions compared to the present method.

## Supplementary material

Videoimages of blood cell deformation during the optical trap experiment as well as movies of three-dimensional computational simulations of the experiments can be seen by accessing the website in the supplementary material provided along with the electronic archive of the companion paper [20].

## Acknowledgements

This work was supported by the Nano Biomechanics Lab, Division of Bioengineering at the National University of Singapore the Laboratory for Experimental and Computational Micromechanics at the Massachusetts Institute of Technology (MIT).

## References

[1] Sheetz MP. Laser tweezers in cell biology. London, UK: Academic Press; 1998.
[2] Henon S, Lenormand G, Richert A, Gallet F. A new determination of the shear modulus of the human erythrocyte membrane using optical tweezers. Biophys J 1999;76:1145–51.
[3] Sleep J, Wilson D, Simmons R, Gratzer W. Elasticity of the red cell membrane and its relation to hemolytic disorders: An optical tweezers study. Biophys J 1999;77:3085–95.

[4] Lenormand G, Henon S, Richert A, Simeon J, Gallet F. Direct measurement of the area expansion and shear moduli of the human red blood cell membrane skeleton. Biophys J 2001;81:43–56.
[5] Kellermayer MSZ, Smith SB, Bustamante C, Granzier HL. Complete unfolding of the titin molecule under external force. J Struct Biol 1998;122:197–205.
[6] Boal D. Mechanics of the cell. Cambridge, UK: Cambridge University Press; 2002.
[7] Rand RP, Burton AC. Mechanical properties of red cell membrane: I. Membrane stiffness and intracellular pressure. Biophys J 1964;4:115–35.
[8] Evans EA. New membrane concept applied to analysis of fluid shear-deformed and micropipet-deformed red blood-cells. Biophys J 1973;13:941–54.
[9] Hochmuth RM, Mohandas N, Blackshe Pl. Measurement of elastic-modulus for red-cell membrane using a fluid mechanical technique. Biophys J 1973;13:747–62.
[10] Zarda PR, Chien S, Skalak R. Elastic deformations of red blood-cells. J Biomech 1977;10:211–21.
[11] Chien S, Sung KLP, Skalak R, Usami S. Theoretical and experimental studies on viscoelastic properties erythrocyte-membrane. Biophys J 1978;24:463–87.
[12] Hochmuth RM, Worthy PR, Evans EA. Red-cell extensional recovery and the determination of membrane viscosity. Biophys J 1979;26:101–14.
[13] Hochmuth RM, Waugh RE. Erythrocyte-membrane elasticity and viscosity. Annu Rev Physiol 1987;49:209–19.
[14] Wu T, Lee GYY, Phan-Thien N, Lim CT. Investigating the mechanical properties of human platelets and erythrocytes using atomic force microscopy. in: International Congress on Biological and Medical Engineering. 2002. Singapore City, Singapore.
[15] Lim HWG, Wortis M, Mukhopadhyay R. Stomatocyte–discocyte–echinocyte sequence of the human red blood cell: evidence for the bilayer-couple hypothesis from membrane mechanics. Proc Natl Acad Sci USA 2002;99:16766–9.
[16] Glenister FK, Coppel RL, Cowman AF, Mohandas N, Cooke BM. Contribution of parasite proteins to altered mechanical properties of malaria-infected red blood cells. Blood 2002;99:1060–3.
[17] Rotsch C, Jacobson K, Radmacher M. Dimensional and mechanical dynamics of active and stable edges in motile fibroblasts investigated by using atomic force microscopy. Proc Natl Acad Sci USA 1999;96:921–6.
[18] Parker KH, Winlove CP. The deformation of spherical vesicles with permeable, constant-area membranes: Application to the red blood cell. Biophys J 1999;77:3096–107.
[19] Fung YC. Biomechanics: mechanical properties of living tissues. 2nd ed. New York, USA: Springer; 1993.
[20] Dao M, Lim CT, Suresh S. Mechanics of human red blood cell deformed by optical tweezers. J Mech Phys Solids 2003;51:2259–80.
[21] Svoboda K, Block SM. Biological applications of optical forces. Biophys J 1994;23:247–85.
[22] Evans EA, Skalak R. Mechanics and thermal dynamics of biomembranes. Boca Raton, FL: CRC Press; 1980.
[23] Simo JC, Pister KS. Remarks on rate constitutive-equations for finite deformation problems - computational implications. Comput Meth Appl Mech Eng 1984;46:201–15.
[24] Hochmuth RM. Properties of red blood cells. In: Skalak R, Chien S, editors. Handbook of bioengineering. New York, USA: McGraw-Hill; 1987.
[25] Evans EA, Hochmuth RM. Membrane viscoelasticity. Biophys J 1976;16:1–11.
[26] Evans EA, Fung YC. Improved measurements of the erythrocyte geometry. Microvasc Res 1972;4:335–47.
[27] ABAQUS, ABAQUS user's manual, version 6.3. Pawtucket, RI, USA: ABAQUS, Inc; 2002.
[28] Discher DE, Mohandas N. Kinematics of red cell aspiration by fluorescence-imaged microdeformation. Biophys J 1996;71:1680–94.
[29] Lim CT, Lee YS, Tan K, Sow CH, Dao M, Suresh S. Work in progress. 2003.
[30] Boey SK, Boal DH, Discher DE. Simulations of the erythrocyte cytoskeleton at large deformation. I. Microscopic models. Biophys J 1998;75:1573–83.
[31] Discher DE, Boal DH, Boey SK. Simulations of the erythrocyte cytoskeleton at large deformation. II. Micropipette aspiration. Biophys J 1998;75:1584–97.
[32] Li J, Dao M, Lim CT, Suresh S. Microscopic models of large deformation of human erythrocyte by optical traps. Manuscript in preparation, 2003.